JACS
JOURNAL OF THE AMERICAN CHEMICAL SOCIETY
pubs.acs.org/JACS
Communication

Spinolate Lanthanide Complexes for High Circularly Polarized Luminescence Metrics in the Visible and Near-Infrared

Bre-Anna N. Willis,[§] David Schnable,[§] Nathan D. Schley, and Gaël Ung*

Cite This: *J. Am. Chem. Soc.* 2022, 144, 22421−22425
Read Online
ACCESS | Metrics & More | Article Recommendations | Supporting Information

ABSTRACT: Analogues of Shibasaki's complexes supported by enantiopure Spinol are synthesized and characterized. The tris(Spinol) Ln^{III} complexes are generated either by ligand deprotonation followed by complexation with lanthanide triflate salts or by in situ deprotonation by $Ln(N(SiMe_3)_2)_3$ salts in the presence of additional base. The resulting complexes are found to be luminescent and chiroptically active for both circular dichroism and circularly polarized luminescence (CPL), notably producing strong CPL with dissymmetry factors (g_{lum}) of up to 0.50, 0.53, and 0.53 for Sm, Tb, and Dy, respectively. The Sm complex is found to be CPL-active in the near-infrared (NIR) region at 980 nm, representing the first report of NIR CPL from Sm. Additionally, the Tb complex, due to efficient sensitization (Φ = 0.846 in tetrahydrofuran) coupled with strong dissymmetry factors, achieves a CPL brightness (B_{CPL}) of 3760 M^{-1} cm^{-1}, the highest reported for any CPL-active compound to date. These are rare examples of compounds that show simultaneous improvement of both CPL metrics (g_{lum} and B_{CPL}). Solid-state structural analysis of the Spinolate complexes and comparisons to other CPL-active analogues of Shibasaki's complexes also suggest that nondistorted geometries should generate even stronger metrics.

Unlocking the potential of circularly polarized luminescence (CPL),[1] the preferential emission of left or right circularly polarized light, requires maximizing two key metrics: the luminescence dissymmetry factor (g_{lum})[2] and the circularly polarized luminescence brightness (B_{CPL}).[3] This would enable key advances in spintronic devices,[4] enhancing security inks,[5] generating three-dimensional displays,[6] and CPL microscopy.[7] The luminescence dissymmetry factor, defined as $g_{lum} = 2(I_L - I_R)/(I_L + I_R)$ (where I_L and I_R are the intensities of the left and right circularly polarized light emitted, respectively) is maximized at ±2, where +2 represents the emission of 100% left circularly polarized light. The CPL brightness is given by $B_{CPL} = \varepsilon_\lambda \Phi |g_{lum}|/2$ (where ε_λ is the extinction coefficient at the excitation wavelength and Φ is the quantum yield) and can essentially be unlimited. Considering these two metrics independently can be misleading, however. For example, high B_{CPL} (418.5 M^{-1} cm^{-1}) can be obtained from strongly absorbing molecular chromium complexes, but their dissymmetry factors are relatively low (g_{lum} = 0.093, representing only 8% preferential polarization),[8] while exceptionally strong dissymmetry factors (g_{lum} = 1.38, ∼81% preferential polarization) can be hampered by weak molar absorptivity and quantum yield (B_{CPL} = 50.7 M^{-1} cm^{-1}).[9] Strategies to maximize both g_{lum} and B_{CPL} *simultaneously* are thus highly desirable.

We have recently shown that lanthanide complexes supported by axially chiral H_8-Binolate ligands provided the highest B_{CPL} reported for terbium (782 M^{-1} cm^{-1}) with a strong g_{lum} of 0.32 (∼28% preferential polarization).[10] We devised a strategy to increase both g_{lum} and B_{CPL} by modifying the twist angle of the chromophore[11] and by improving the quantum yield by rigidifying the ligand,[12] respectively. We chose 1,1′-spirobiindane-7,7′-diol (Spinol) (Scheme 1) as a potential ligand because the presence of the spiro sp^3 carbon prevents the rotation of the two phenol planes. We show below that Spinolate−lanthanide complexes are accessible synthetically and provide strong metrics for circularly polarized luminescence. For example, the highest reported g_{lum} (0.53, ∼42% preferential polarization) for a terbium complex was obtained along with the highest B_{CPL} (3760 M^{-1} cm^{-1}) reported for any molecule to date. Additionally, strong CPL metrics from a samarium complex in the near-infrared (NIR) region were obtained for the first time.

Scheme 1. Synthesis of $[(R\text{-Spinol})_3LnNa_3(thf)_6]$ (Ln = Sm, Eu, Tb, Dy)[a]

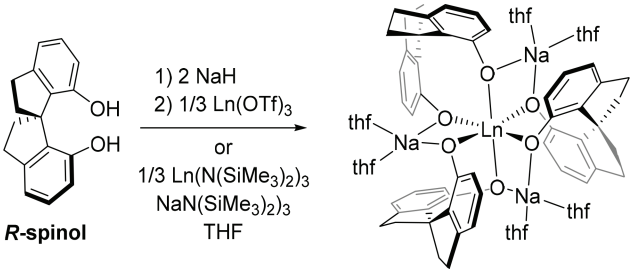

[a]The synthesis of the enantiomeric complexes was done analogously starting from *S*-Spinol.

Received: September 28, 2022
Published: November 29, 2022

https://doi.org/10.1021/jacs.2c10364
J. Am. Chem. Soc. 2022, 144, 22421−22425

Despite its extensive use as a chiral scaffold, for example as chiral phosphoric acids,[13] diphosphines,[14] phosphoramidite,[15] or phosphoramide,[16] Spinol has not been investigated in the coordination chemistry of the lanthanides to date. Inspired by our work on lanthanides supported by axially chiral ligands,[10,17] we synthesized the complexes $[(Spinol)_3LnNa_3(thf)_6]$ (Ln = Sm, Eu, Tb, Dy) either by salt metathesis utilizing sodium Spinolate and lanthanide trifluoromethanesulfonate salts or by the reaction of 3 equiv of Spinol with $Ln(N(SiMe_3)_2)_3$ in the presence of 3 equiv of $NaN(SiMe_3)_2$. (Scheme 1) After workup, the complexes were recrystallized from THF. Despite some paramagnetic broadening and shifting, the ^{1}H NMR spectra of the complexes unequivocally indicated the presence of a unique C_3-symmetric species in solution (Figures S3–S7). Single crystals of $[(R\text{-}Spinol)_3EuNa_3(thf)_6]$ were grown from slow diffusion of pentane into a saturated THF solution. The compound crystallized in the noncentrosymmetric space group $P2_12_12_1$. Single-crystal X-ray diffraction studies showed that the europium is six-coordinate, in a highly distorted octahedral geometry (Figure 1). The ligands are arranged in a propeller with Λ chirality. The sodium cations bridge the Spinolate ligands and are further ligated with two THF molecules.

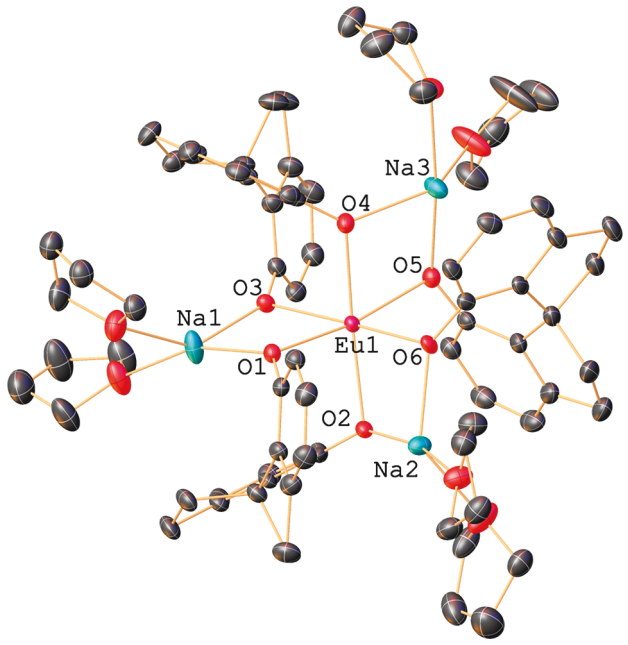

Figure 1. Structure of $[(R\text{-}Spinol)_3EuNa_3(thf)_6]$ in the solid state. Thermal ellipsoids are drawn at 50% probability. Hydrogen atoms have been omitted for clarity.

The $[(R\text{-}Spinol)_3EuNa_3(thf)_6]$ complex did not display the typical luminescence expected from Eu^{3+} ions at room temperature. This is reminiscent of the results observed using H_8-Binol[10] and may be due to quenching from low-lying ligand-to-metal charge transfer (LMCT) states or photoinduced electron transfer (PeT) to the mildly oxidizing europium. These phenomena have been observed in similarly electron-rich antennae.[18] Luminescence was observed in a frozen 2-methyltetrahydrofuran glass at 77 K (Figure S15), further confirming deactivation of the ligand excited state at room temperature via an LMCT or PeT process.[12] Nevertheless, the samarium, terbium, and dysprosium analogues all displayed typical lanthanide luminescence at room temperature (Figures S9, S8, and S10, respectively) with good to excellent quantum yields (2.8%, 84.6%, and 15.5%, respectively). The low quantum yield of the samarium complex is likely due to a combination of its ladderlike electronic structure facilitating nonradiative decay pathways[19] and a quenching pathway similar to but lessened compared with that in the europium complex, since samarium[20] is typically slightly less oxidizing than europium.[21] Despite the low quantum efficiency, relatively strong samarium emission in the NIR was still observed (Figure S9). Several factors contribute to the much stronger quantum yield observed for the terbium complexes compared to their H_8-Binol analogues. First, the excited triplet energy level of Spinol (obtained from low-temperature phosphorescence of the analogous gadolinium complex; see Figure S15) is slightly higher (~2400 cm^{-1}) than the triplet energy level of H_8-Binol, reducing the energy back-transfer from the terbium excited state. Additionally, the singlet energy level of Spinol is also higher than that of H_8-Binol (~2000 cm^{-1}; Figure S15), allowing better energy transfer to higher excited-state levels of terbium, a phenomenon previously observed in other highly efficient phenol-supported terbium emitters.[12] Lastly, the higher quantum yield can also be attributed to the significantly increased rigidity caused by the spiro carbon of Spinol and lower vibrational quenching.[12] Long lifetimes (69.4, 1180, and 70.9 μs for Sm, Tb, and Dy, respectively), consistent with typical lanthanide luminescence, were measured. The decays were found to be monoexponential, confirming the presence of one major emissive species in solution.

Circularly polarized luminescence spectra of the $[(Spinol)_3SmNa_3(thf)_6]$ complexes were obtained in dilute THF solutions (7.1 × 10^{-4} mol L^{-1}) (Figure 2). Strong to very

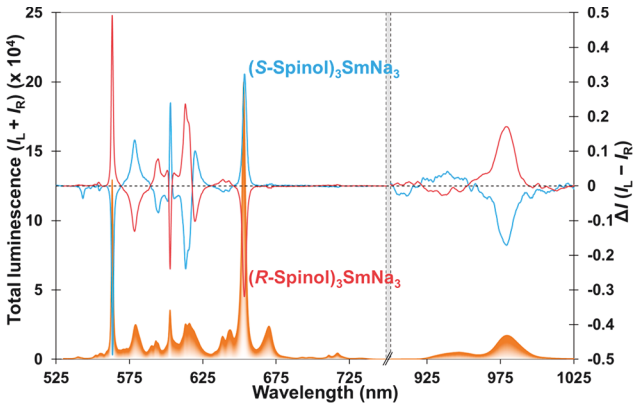

Figure 2. CPL spectra of $[(R\text{-}Spinol)_3SmNa_3(thf)_6]$ (red) and $[(S\text{-}Spinol)_3SmNa_3(thf)_6]$ (blue) in tetrahydrofuran solutions (7.1 × 10^{-4} mol L^{-1}) at room temperature. See Figure S18 for the g_{lum} plot. Total luminescence is traced in the background. Excitation at 295 nm. Bandpass: 0.5 nm in the visible and 13 nm in the NIR. The gray area was not measured.

strong dissymmetry factors (0.20, 0.50, and 0.12) were obtained for the visible transitions $^4G_{5/2} \rightarrow {}^6H_J$ (J = 5/2, 7/2, and 9/2, respectively) and are among the stronger dissymmetry factors reported to date for samarium complexes. The CPL brightnesses obtained for our samarium complex are compiled in Table 1 and are comparable to those of other strong samarium emitters (see the Supporting Information for a discussion of B_{CPL} calculations for lanthanide emitters).[10,22]

https://doi.org/10.1021/jacs.2c10364
J. Am. Chem. Soc. 2022, 144, 22421−22425

Table 1. Summary of the Photophysical Properties of $[(Spinol)_3LnNa_3(thf)_6]$

Ln	λ (nm)	ε (295 nm) (M^{-1} cm^{-1})	Φ	transition	$\lvert g_{lum}\rvert$	B_{CPL} (M^{-1} cm^{-1})
Sm	565	21160	0.028	$^4G_{5/2} \rightarrow {}^6H_{5/2}$	0.20	6.1
	610			$^4G_{5/2} \rightarrow {}^6H_{7/2}$	0.50	19.0
	655			$^4G_{5/2} \rightarrow {}^6H_{9/2}$	0.12	14.2
	980			$^4G_{5/2} \rightarrow {}^6F_{5/2}$	0.17	6.9
Tb	490	24460	0.846	$^5D_4 \rightarrow {}^7F_6$	0.40	680
	545			$^5D_4 \rightarrow {}^7F_5$	0.53	3760
	595			$^5D_4 \rightarrow {}^7F_4$	0.38	275
	635			$^5D_4 \rightarrow {}^7F_3$	0.43	477
Dy	475	19790	0.155	$^4F_{9/2} \rightarrow {}^6H_{15/2}$	0.24	22.0
	590			$^4F_{9/2} \rightarrow {}^6H_{13/2}$	0.07	86.9
	670			$^4F_{9/2} \rightarrow {}^6H_{11/2}$	0.36	28.2
	760			$^4F_{9/2} \rightarrow {}^6H_{9/2}$	0.53	33.9

The strong luminescence component in the NIR region allowed us to measure a reliable CPL spectrum from 850 to 1250 nm. While no detectable CPL was observed for the $^4G_{5/2} \rightarrow {}^6F_J$ (J = 7/2 and 9/2) transitions at 1060 and 1230 nm, strong CPL was observed at 940 and 980 nm ($|g_{lum}|$ = 0.10 and 0.17, respectively). This is the first time that NIR CPL from samarium is reported. The peak at 980 nm can be unambiguously attributed to the $^4G_{5/2} \rightarrow {}^6F_{5/2}$ transition, while the peak at 940 nm is likely a combination of the $^4G_{5/2} \rightarrow {}^6F_J$ (J = 1/2, 3/2) and $^4G_{5/2} \rightarrow {}^6H_{13/2}$ transitions. The strength of the CPL signal obtained is likely due to the contribution of the $^4G_{5/2} \rightarrow {}^6F_{3/2}$ transition, considering its predicted rotatory strength.[23] The CPL brightness in the NIR is 6.9 M^{-1} cm^{-1}, which is comparable to those of many ytterbium-based CPL-NIR emitters.[3b]

Circularly polarized luminescence spectra of the $[(Spinol)_3TbNa_3(thf)_6]$ complexes were obtained in dilute THF solutions (7.1×10^{-4} mol L^{-1}) (Figure 3). The overall shape

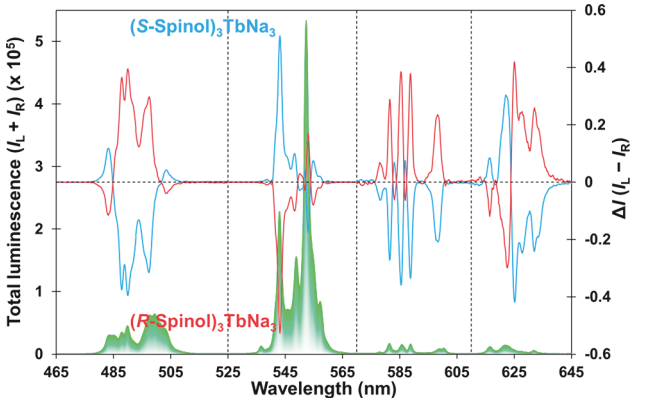

Figure 3. CPL spectra of $[(R\text{-Spinol})_3TbNa_3(thf)_6]$ (red) and $[(S\text{-Spinol})_3TbNa_3(thf)_6]$ (blue) in tetrahydrofuran solutions (7.1×10^{-4} mol L^{-1}) at room temperature. See Figure S19 for the g_{lum} plot. Total luminescence is traced in the background. Excitation at 295 nm. Bandpass: 0.5 nm.

of the CPL signals is reminiscent of those of the H_8-Binol-supported terbium complex, which indicates that their solution structures must be similar. However, significantly stronger dissymmetry factors were obtained. The $^5D_4 \rightarrow {}^7F_J$ (J = 6, 5, 4, 3) transitions exhibited $|g_{lum}|$ = 0.40, 0.53, 0.38, and 0.43, respectively, which represent the highest dissymmetry factors observed for any terbium complexes to date. These numbers translate to CPL brightnesses of up to 3760 M^{-1} cm^{-1} (Table 1), the highest number ever reported for any CPL-active compound.

The $[(Spinol)_3DyNa_3(thf)_6]$ complexes also exhibited strong dissymmetry factors in the visible region ($|g_{lum}|$ = 0.24 and 0.36 at 475 and 670 nm, respectively) (Figure 4). A very

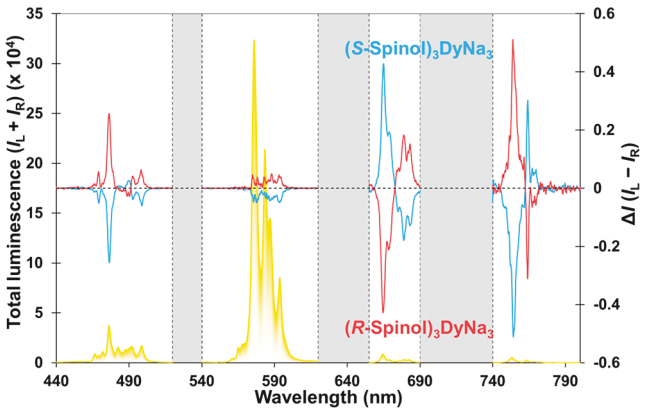

Figure 4. CPL spectra of $[(R\text{-Spinol})_3DyNa_3(thf)_6]$ (red) and $[(S\text{-Spinol})_3DyNa_3(thf)_6]$ (blue) in tetrahydrofuran solutions (7.1×10^{-4} mol L^{-1}) at room temperature. See Figure S20 for the g_{lum} plot. Total luminescence is traced in the background. Excitation at 295 nm. Bandpass: 0.5 nm. Gray areas were not measured.

strong dissymmetry factor of 0.53 was observed for the $^4F_{9/2} \rightarrow {}^6H_{9/2}$ transition in the far-red (765 nm), which is the highest dissymmetry factor for dysprosium reported to date. While still the strongest observed to date, the CPL brightness values (up to 86.9 M^{-1} cm^{-1}) are still modest due to the fact that the most luminescent transition ($^4F_{9/2} \rightarrow {}^6H_{13/2}$ at 590 nm) displays a very weak dissymmetry factor ($|g_{lum}|$ = 0.05). Future synthetic efforts should be directed toward modifying the symmetry and ligand field to enhance the dissymmetry factor of this transition and compensate for the less CPL-favorable selection rules of this transition.[23]

We sought structural insights to draw hypotheses explaining the high metrics obtained. We thus compared the octahedra formed by the H_8-Binolate and Spinolate ligands. Deviations of the O−Ln−O angle, given by the Σ parameter, and distortion from octahedral to trigonal-prismatic, given by the Θ parameter, were calculated from the solid-state structures.[24] While the structure is still significantly distorted, both the Σ and Θ values are closer to those for a perfect octahedron in

https://doi.org/10.1021/jacs.2c10364
J. Am. Chem. Soc. 2022, 144, 22421−22425

$[(Spinol)_3LnNa_3(thf)_6]$ compared to $[(H_8\text{-Binol})_3LnNa_3(thf)_6]$ (Σ = 126.7° vs 137.0° and Θ = 364° vs 378°, respectively). In the complexes, the planes of the phenolate moieties of H_8-Binol and Spinol are virtually superimposed, while a slight change in the C_{Ar}–O–Ln angle (16°) is observed. The latter impacts the orientation and strength of the electric dipole transition moment, which potentially also positively affects the dissymmetry factors. This suggests that a *nondistorted* octahedral geometry, combined with properly engineered chromophore angles, would generate stronger dissymmetry factors. This is consistent with the fact that the highest dissymmetry factor to date was also obtained in a *nondistorted* eight-coordinate geometry in $[Eu(hfbc)_4]$-[Cs], which exhibits a perfect square-antiprism geometry.[25]

We have successfully coordinated Spinol to lanthanide ions, yielding Spinol-supported analogues of the well-known Shibasaki complexes. Given the performances of the latter in asymmetric catalysis,[26] our complexes could be investigated in this context in the future. More importantly, we have obtained some of the highest reported circularly polarized luminescence metrics to date. Dissymmetry factors of up to 0.50, 0.53, and 0.53 were obtained for Sm, Tb, and Dy, respectively, yielding the highest CPL brightness reported to date (3760 M^{-1} cm^{-1} for Tb). Our structural analysis suggests that even higher metrics could be obtained for a perfect octahedral geometry for six-coordinate species associated with chromophores with an appropriate angle and strength of their electric dipole transition moment. Designing and exploring other phenolate-based axially chiral ligands with the proper bite angle to achieve such goals would thus be highly beneficial and will be one of the focuses of our group.

■ ASSOCIATED CONTENT

Supporting Information

The Supporting Information is available free of charge at https://pubs.acs.org/doi/10.1021/jacs.2c10364.

Experimental details, supplemental spectra (UV–vis, CPL, CD, NMR), crystallographic parameters, and tabulated photophysical measurements (PDF)

Accession Codes

CCDC 2208146 contains the supplementary crystallographic data for this paper. These data can be obtained free of charge via www.ccdc.cam.ac.uk/data_request/cif, or by emailing data_request@ccdc.cam.ac.uk, or by contacting The Cambridge Crystallographic Data Centre, 12 Union Road, Cambridge CB2 1EZ, U.K.; fax: +44 1223 336033.

■ AUTHOR INFORMATION

Corresponding Author

Gaël Ung – *Department of Chemistry, University of Connecticut, Storrs, Connecticut 06269, United States;* orcid.org/0000-0002-6313-3658; Email: gael.ung@uconn.edu

Authors

Bre-Anna N. Willis – *Department of Chemistry, University of Connecticut, Storrs, Connecticut 06269, United States*

David Schnable – *Department of Chemistry, University of Connecticut, Storrs, Connecticut 06269, United States;* orcid.org/0000-0002-8650-997X

Nathan D. Schley – *Department of Chemistry, Vanderbilt University, Nashville, Tennessee 37235, United States;* orcid.org/0000-0002-1539-6031

Complete contact information is available at: https://pubs.acs.org/10.1021/jacs.2c10364

Author Contributions

§B.-A.N.W. and D.S. contributed equally.

Notes

The authors declare no competing financial interest.

■ ACKNOWLEDGMENTS

This material is based upon work supported by the National Science Foundation under Grant CHE-2041084. B.-A.N.W. and G.U. thank the National Science Foundation for supporting the UConn Chemistry REU Program under Grant CHE-1757634. The authors acknowledge Dr. Tomoyasu Mani for assistance in the collection of low-temperature emission data.

■ REFERENCES

(1) (a) Sánchez-Carnerero, E. M.; Agarrabeitia, A. R.; Moreno, F.; Maroto, B. L.; Muller, G.; Ortiz, M. J.; de la Moya, S. Circularly Polarized Luminescence from Simple Organic Molecules. *Chem. - Eur. J.* **2015**, *21* (39), 13488–13500. (b) Zinna, F.; di Bari, L. Lanthanide Circularly Polarized Luminescence: Bases and Applications. *Chirality* **2015**, *27*, 1–13. (c) Carr, R.; Evans, N. H.; Parker, D. Lanthanide Complexes as Chiral Probes Exploiting Circularly Polarized Luminescence. *Chem. Soc. Rev.* **2012**, *41* (23), 7673–7686. (d) Muller, G. Luminescent Chiral Lanthanide(III) Complexes as Potential Molecular Probes. *Dalton Trans.* **2009**, No. 44, 9692. (e) Dhbaibi, K.; Favereau, L.; Crassous, J. Enantioenriched Helicenes and Helicenoids Containing Main-Group Elements (B, Si, N, P). *Chem. Rev.* **2019**, *119* (14), 8846–8953.

(2) Riehl, J. P.; Richardson, F. S. Circularly Polarized Luminescence Spectroscopy. *Chem. Rev.* **1986**, *86* (1), 1–16.

(3) (a) Nagata, Y.; Mori, T. Irreverent Nature of Dissymmetry Factor and Quantum Yield in Circularly Polarized Luminescence of Small Organic Molecules. *Front. Chem.* **2020**, *8*, 448. (b) Arrico, L.; di Bari, L.; Zinna, F. Quantifying the Overall Efficiency of Circularly Polarized Emitters. *Chem. - Eur. J.* **2021**, *27* (9), 2920–2934.

(4) (a) Farshchi, R.; Ramsteiner, M.; Herfort, J.; Tahraoui, A.; Grahn, H. T. Optical Communication of Spin Information between Light Emitting Diodes. *Appl. Phys. Lett.* **2011**, *98* (16), 162508. (b) Sherson, J. F.; Krauter, H.; Olsson, R. K.; Julsgaard, B.; Hammerer, K.; Cirac, I.; Polzik, E. S. Quantum Teleportation between Light and Matter. *Nature* **2006**, *443* (7111), 557–560.

(5) MacKenzie, L. E.; Pal, R. Circularly Polarized Lanthanide Luminescence for Advanced Security Inks. *Nat. Rev. Chem.* **2021**, *5*, 109–124.

(6) Schadt, M. Liquid Crystal Materials and Liquid Crystal Displays. *Annu. Rev. Mater. Sci.* **1997**, *27* (1), 305–379.

(7) Stachelek, P.; MacKenzie, L.; Parker, D.; Pal, R. Circularly Polarised Luminescence Laser Scanning Confocal Microscopy to Study Live Cell Chiral Molecular Interactions. *Nat. Commun.* **2022**, *13* (1), 1–8.

(8) Dee, C.; Zinna, F.; Kitzmann, W. R.; Pescitelli, G.; Heinze, K.; di Bari, L.; Seitz, M. Strong Circularly Polarized Luminescence of an Octahedral Chromium(III) Complex. *Chem. Commun.* **2019**, *55* (87), 13078–13081.

(9) Lunkley, J. L.; Shirotani, D.; Yamanari, K.; Kaizaki, S.; Muller, G. Extraordinary Circularly Polarized Luminescence Activity Exhibited by Cesium Tetrakis(3-heptafluoro-butylryl-(+)-camphorato) Eu(III) Complexes in EtOH and $CHCl_3$ Solutions. *J. Am. Chem. Soc.* **2008**, *130* (42), 13814–13815.

(10) Deng, M.; Schley, N. D.; Ung, G. High Circularly Polarized Luminescence Brightness from Analogues of Shibasaki's Lanthanide Complexes. *Chem. Commun.* **2020**, *56* (94), 14813−14816.
(11) di Pietro, S.; di Bari, L. The Structure of $MLn(Hfbc)_4$ and a Key to High Circularly Polarized Luminescence. *Inorg. Chem.* **2012**, *51* (21), 12007−12014.
(12) Aquino, L. E. d. N.; Barbosa, G. A.; Ramos, J. d. L.; Giese, S. O. K.; Santana, F. S.; Hughes, D. L.; Nunes, G. G.; Fu, L.; Fang, M.; Poneti, G.; Carneiro Neto, A. N.; Moura, R. T.; Ferreira, R. A. S.; Carlos, L. D.; Macedo, A. G.; Soares, J. F. Seven-Coordinate Tb^{3+} Complexes with 90% Quantum Yields: High-Performance Examples of Combined Singlet- and Triplet-to-Tb^{3+} Energy-Transfer Pathways. *Inorg. Chem.* **2021**, *60* (2), 892−907.
(13) (a) Gelis, C.; Bekkaye, M.; Lebée, C.; Blanchard, F.; Masson, G. Chiral Phosphoric Acid Catalyzed [3 + 2] Cycloaddition and Tandem Oxidative [3 + 2] Cycloaddition: Asymmetric Synthesis of Substituted 3-Aminodihydrobenzofurans. *Org. Lett.* **2016**, *18* (14), 3422−3425. (b) Li, S.; Zhang, J. W.; Li, X. L.; Cheng, D. J.; Tan, B. Phosphoric Acid-Catalyzed Asymmetric Synthesis of SPINOL Derivatives. *J. Am. Chem. Soc.* **2016**, *138* (50), 16561−16566.
(14) Endo, K.; Hamada, D.; Yakeishi, S.; Ogawa, M.; Shibata, T. Multinuclear Cu-Catalysts Based on SPINOL-PHOS in Asymmetric Conjugate Addition of Organozinc Reagents. *Org. Lett.* **2012**, *14* (9), 2342−2345.
(15) Wang, K.; Lin, X.; Li, Q.; Liu, Y.; Li, C. The Synthesis of Tetracyclic Coumarins via Decarboxylative Asymmetric [4 + 2] Cycloadditions Enabled by Pd(0)/Cu(I) Synergistic Catalysis. *Chin. J. Catal.* **2022**, *43* (7), 1812−1817.
(16) Zhuang, M.; Du, H. Asymmetric Rearrangement of Racemic Epoxides Catalyzed by Chiral Brønsted Acids. *Org. Biomol. Chem.* **2013**, *11* (9), 1460−1462.
(17) Mukthar, N. F. M.; Schley, N. D.; Ung, G. Strong Circularly Polarized Luminescence at 1550 Nm from Enantiopure Molecular Erbium Complexes. *J. Am. Chem. Soc.* **2022**, *144* (14), 6148−6153.
(18) (a) Kovacs, D.; Borbas, K. E. The Role of Photoinduced Electron Transfer in the Quenching of Sensitized Europium Emission. *Coord. Chem. Rev.* **2018**, *364*, 1−9. (b) Miranda, Y. C.; Pereira, L. L. A. L.; Barbosa, J. H. P.; Brito, H. F.; Felinto, M. C. F. C.; Malta, O. L.; Faustino, W. M.; Teotonio, E. E. S. The Role of the Ligand-to-Metal Charge-Transfer State in the Dipivaloylmethanate-Lanthanide Intramolecular Energy Transfer Process. *Eur. J. Inorg. Chem.* **2015**, *2015* (18), 3019−3027. (c) Kovacs, D.; Mathieu, E.; Kiraev, S. R.; Wells, J. A. L.; Demeyere, E.; Sipos, A.; Borbas, K. E. Coordination Environment-Controlled Photoinduced Electron Transfer Quenching in Luminescent Europium Complexes. *J. Am. Chem. Soc.* **2020**, *142* (30), 13190−13200.
(19) Bünzli, J.-C. G.; Eliseeva, S. V. Basics of Lanthanide Photophysics. In *Lanthanide Luminescence*; Hänninen, P.; Härmä, H., Eds.; Springer, 2011.
(20) Szostak, M.; Spain, M.; Procter, D. J. Determination of the Effective Redox Potentials of SmI_2, $SmBr_2$, $SmCl_2$, and Their Complexes with Water by Reduction of Aromatic Hydrocarbons. Reduction of Anthracene and Stilbene by Samarium(II) Iodide-Water Complex. *J. Org. Chem.* **2014**, *79* (6), 2522−2537.
(21) Bratsch, S. G. Standard Electrode Potentials and Temperature Coefficients in Water at 298.15 K. *J. Phys. Chem. Ref. Data* **1989**, *18* (1), 1−21.
(22) (a) Ayers, K. M.; Schley, N. D.; Ung, G. Circularly Polarized Luminescence from Enantiopure C_2-Symmetrical Tetrakis(2-pyridylmethyl)-1,2-diaminocyclohexane Lanthanide Complexes. *Inorg. Chem.* **2020**, *59* (11), 7657−7665. (b) Schnable, D.; Freedman, K.; Ayers, K. M.; Schley, N. D.; Kol, M.; Ung, G. Synthesis of Enantiopure Lanthanide Complexes Supported by Hexadentate *N*,*N*′-Bis(methylbipyridyl)bipyrrolidine and Their Circularly Polarized Luminescence. *Inorg. Chem.* **2020**, *59* (12), 8498−8504.
(23) Richardson, F. S. Selection Rules for Lanthanide Optical Activity. *Inorg. Chem.* **1980**, *19* (9), 2806−2812.
(24) Ketkaew, R.; Tantirungrotechai, Y.; Harding, P.; Chastanet, G.; Guionneau, P.; Marchivie, M.; Harding, D. J. OctaDist: A Tool for Calculating Distortion Parameters in Spin Crossover and Coordination Complexes. *Dalton Trans.* **2021**, *50* (3), 1086−1096.
(25) Lunkley, J. L.; Shirotani, D.; Yamanari, K.; Kaizaki, S.; Muller, G. Chiroptical Spectra of a Series of Tetrakis((+)-3-Heptafluorobutylyrylcamphorato)Lanthanide(III) with an Encapsulated Alkali Metal Ion: Circularly Polarized Luminescence and Absolute Chiral Structures for the Eu(III) and Sm(III) Complexes. *Inorg. Chem.* **2011**, *50* (24), 12724−12732.
(26) (a) Shibasaki, M.; Kanai, M.; Matsunaga, S.; Kumagai, N. Recent Progress in Asymmetric Bifunctional Catalysis Using Multimetallic Systems. *Acc. Chem. Res.* **2009**, *42* (8), 1117−1127. (b) Panetti, G. B.; Robinson, J. R.; Schelter, E. J.; Walsh, P. J. Expanding the Rare-Earth Metal BINOLate Catalytic Multitool beyond Enantioselective Organic Synthesis. *Acc. Chem. Res.* **2021**, *54* (11), 2637−2648. (c) Shibasaki, M.; Yoshikawa, N. Lanthanide Complexes in Multifunctional Asymmetric Catalysis. *Chem. Rev.* **2002**, *102* (6), 2187−2209.

https://doi.org/10.1021/jacs.2c10364
J. Am. Chem. Soc. 2022, 144, 22421−22425